Institutionen för medicin och vård
Avdelningen för radiofysik
Hälsouniversitetet

The Linogram Algorithm and Direct Fourier Method with Linograms

Paul R. Edholm

Department of Medicine and Care
Radio Physics
Faculty of Health Sciences

Series: Report / Institutionen för radiologi, Universitetet i Linköping; 65
ISSN: 1102-1799
ISRN: LIU-RAD-R-065

Publishing year: 1991

1991-01-22 ISSN 0348-7679

The Linogram Algorithm and Direct Fourier Method with Linograms

Paul R. Edholm

Avdelningen för diagnostisk radiologi
Universitetet i Linköping

REPORT
ULI-RAD-R-065

The Linogram Algorithm and Direct Fourier Method with Linograms

Paul R. Edholm

The conventional map of projection data will here be called the sinogram map. Among the algorithms used with this map of data there are two of main interest for this paper: the Filtered Back Projection (FBP) and the Direct Fourier Method (DFM). FBP is the most popular algorithm used in commercial CT machines although it is computationally expensive compared to the DFM. The reason for its popularity is that FBP gives better pictures than the DFM unless the latter is used with very careful interpolations.

In this paper another map of projection data will be presented, here called the linogram map. The FBP may be implemented with this map in a particularly simple way, here called the Linogram Algorithm (LA). In this the back projection, which is so computationally expensive with the sinogram map, can be reduced to a computationally inexpensive series of FFT's.

The DFM may also be implemented with the linogram map in a particular way so that it turns out that the two methods FBP and the DFM are computationally identical.

The LA has been described in [1-5]. In [4] a definition of linograms was introduced, which is slightly different from the definition given in [1-3], and leads to a somewhat simplified mathematical description of the algorithm.

This text is an attempt to describe the Linogram Algorithm based on some of the ideas in [4] and also such that the mathematical description is more similar to the actual digital implementation.

The DFM method with linograms will also be presented. The two methods, which are different conceptually, have a very similar structure. In both the image is reconstructed without any interpolations.

Geometry. Let the object to be reconstructed be the function $\underline{f}: R^2 \to R$, such that

$$f(x,y) = \begin{cases} 0 \text{ for } |x| \geq 1 \text{ or } |y| \geq 1 \\ \geq 0 \text{ otherwise .} \end{cases} \qquad (1)$$

In image reconstruction from projections it is necessary to specify line integrals through the plane of the object, i.e. projecting rays in all possible directions. A line through the object may be specified by two coordinates. Based on the geometry of the detector array, the usual way is to let the first coordinate define the length of the normal to the line from the origin, and the second coordinate the angle from the x-axis to this normal in the counterclockwise direction. If these coordinates are (r_p, Θ_p), then the line through the (x,y)-plane has the equation

$$r_p = x \cos\Theta_p + y \sin\Theta_p \ . \tag{2}$$

All possible lines in the (x,y)-plane may be specified in this way. In the plane of the rectangular coordinate system (r, Θ), each point defines a line through the (x, y)-plane, (Fig 1) which may be written

$$x = r/(\cos\Theta) - y \tan\Theta \tag{3}$$

The point (x_p, y_p) in the (x,y)-plane defines the sinusoid

$$r = x_p \cos\Theta + y_p \sin\Theta \tag{4}$$

in the (r,Θ)-plane. If we now have chosen (x_p,y_p) so that this point is on the line (2) in the (x,y)-plane, the sinusoid (4) must pass through the point (r_p,Θ_p), which represents all points on (2) (Fig 2). The other points on this sinusoid define all other lines in the (x,y)-plane passing through the point (x_p,y_p). This is seen by inserting (4) in (3)

$$x = (x_p \cos\Theta + y_p \sin\Theta)/\cos\Theta - y \tan\Theta$$

or

$$x = x_p + (y_p - y) \tan\Theta \ . \tag{5}$$

When Θ varies through the range π, the expression (5) describes all lines in the (x,y)-plane passing through (x_p,y_p).

A line through the (x,y)-plane may be specified by a number of ways. Is it possible to find another coordinate system, say (u, v), in which, as before, every point defines a line through the (x, y)-plane and also such that the set of points defining all lines through a specific point (x_p, y_p) instead of a sinusoid, forms a straight line in the (u, v)-plane?

Define a line in the x,y-plane as

$$x = u_p - yv_p \quad , \tag{6}$$

where (u_p, v_p) is a specific point in the (u, v)-plane (Fig 3). The points in the (u,v)-plane defines all possible lines through the (x,y)-plane

$$x = u - yv \quad . \tag{7}$$

Assume that our previous point, (x_p, y_p), is a point somewhere on the line (6), then

$$u = x_p + y_p v \quad , \tag{8}$$

is a straight line through the (u, v)-plane (Fig 4). As we have chosen (x_p,y_p) to be on the line (6) in the (x,y)-plane, the line (8) in the (u,v)-plane must pass through (u_p, v_p), which represents all points on (6). The other points on this line define all other lines in the (x, y)-plane passing through (x_p, y_p).

This may be seen by inserting (8) in (7).

$$x = (x_p + y_p v) - yv \quad ,$$

or

$$x = x_p + (y_p - y)\, v \quad . \tag{9}$$

When v varies from $-\infty$ to ∞, the expression (9) describes all lines in the (x,y)-plane passing through (x_p, y_p).

There is a kind of symmetry between the (x,y) and the (u,v) systems as is seen by (6) and (8). A point in one system defines a line in the other.

Sinograms and Linograms. When projection data, in the form of line integrals through a function f(x,y), are mapped in the (r,Θ)-coordinates, where data for a point in the object form the sinusoid (4), this map is usually called a sinogram [6], and it may be denoted $p(r,\Theta)$ and defined as

$$p(r,\Theta) = \int_{-\infty}^{\infty} f(r\cos\Theta - t\sin\Theta,\ r\sin\Theta + t\cos\Theta)dt \tag{10}$$

If the projection data instead are mapped in the (u,v) coordinates where data for a point in the object form the straight line (8), this map will be called a linogram analogous to the term sinogram [1].

Why linograms instead of sinograms? Well, in the most popular algorithm, called filtered back projection, the projection data are first subjected to a filtration of their spatial frequencies and then "back projected". This is a somewhat unprecise expression. The mathematical definition is that each point in the object is reconstructed by making an integration of the filtered projection data representing all line integrals through the point in question.

In the sinogram case we then have to do an integration along a sinusoid for each point, but in the linogram case this integration is along a straight line. This may be a simpler operation, and as we will see later, the use of linograms allows us to replace the computationally expensive back projection by a series of fast Fourier transforms.

The relation between the coordinates for the sinogram (r,Θ) and the linogram (u,v) are

$$\begin{cases} r = \dfrac{u}{\sqrt{(1+v^2)}} \\ \Theta = \arctan v, \end{cases} \qquad \text{or} \qquad \begin{aligned} u &= \frac{r}{\cos\Theta} \\ v &= \tan\Theta \end{aligned} \quad .$$

Linograms. A linogram mapping all lines through $f(x,y)$ has to have a range in v from $-\infty$ to ∞, corresponding to a range of π for Θ in the sinogram. In order to have a finite range for v we are going to use two finite linograms.

The first will be called $g_0(u, v)$ and contains projection data of $f(x, y)$ for the range $-1 \leqslant v < 1$.

The second will be called $g_1(u, v)$ and is achieved by first rotating the object clockwise the angle $\frac{\pi}{2}$ and then taking projections of it for the range $-1 \leqslant v < 1$, exactly as for $g_0(u, v)$.

From the two linograms two partial images will be reconstructed, $f_0(x, y)$ and $f_1(x, y)$. The final image is formed by first rotating $f_1(x,y)$ counterclockwise the angle $\pi/2$ and then adding it to $f_0(x,y)$.

Let Q define a counterclockwise rotation the angle $\pi/2$ of a function $f:R^2 \rightarrow R$ around the origin so that

$$\begin{aligned} [Q^1 f]\ (x,\ y) &= f\ (-y,\ x), \\ [Q^0 f]\ (x,\ y) &= f\ (x,\ y) \text{ and} \\ [Q^{-1} f]\ (x,\ y) &= f\ (y,\ -x). \end{aligned} \tag{11}$$

For any 2-dimensional function $\underline{f}$ we use, respectively, $F^{[1]}\underline{f}$, $F^{[2]}\underline{f}$ and $F_2\underline{f}$ to denote the Fourier transform of $\underline{f}$ with respect to its first variable, the Fourier transform of $\underline{f}$ with respect to its second variable, and the two-dimensional Fourier transform of $\underline{f}$. Variables in the spatial domain are represented by small letters and in the Fourier domain by capital letters.

In the following expressions, k is an index assuming the two values 0 and 1. The range of v is limited to $-1 \leqslant v < 1$. The two linograms g_0 and g_1 are then defined by

$$g_k\ (u,v) = \int_{-\infty}^{\infty} [Q^{-k} f]\ (u-yv,y)\ dy\ ;\ k=0,1;\quad -1 \leqslant v < 1. \tag{12}$$

The RHS represents line integrals through f(x,y), where x has been replaced by (u-yv) according to (7).

<u>The filter</u>. The linograms defined by (12) cannot be used directly for reconstruction, they have first to be filtered.

We will now try to find how to make a proper filtration of the spatial frequencies of the projection data in the linogram. As a preliminary we will first make an 1-dimensional Fourier transform of g_k in the first variable

$$[F^{[1]} g_k]\ (U,\ v) = \int_{-\infty}^{\infty} g_k\ (u,\ v)\ e^{-i2\pi\ Uu} du\ . \tag{13}$$

Insert (12) in (13)

$$[F^{[1]} g_k]\ (U,\ v) = \int_{-\infty}^{\infty} \left\{ \int_{-\infty}^{\infty} [Q^{-k} f]\ (u-yv,\ y)\ dy \right\} e^{-i2\pi\ Uu} du\ . \tag{14}$$

Change variabel from u to x

$$\begin{cases} x = u - yv \\ u = x + yv \end{cases} ; \quad \frac{dx}{du} = 1 \tag{15}$$

$$[F^{[1]}g_k]\ (U,\ v) = \int_{-\infty}^{\infty} \left\{ \int_{-\infty}^{\infty} [Q^{-k}f]\ (x,\ y)\ dy \right\} e^{-i2\pi\ U\ (x+yv)} dx$$

$$= \int_{-\infty}^{\infty} \int_{-\infty}^{\infty} [Q^{-k}f]\ (x,\ y)\ e^{-i2\pi\ U\ (x+yv)}\ dxdy. \tag{16}$$

The LHS of (16) is a 1-D Fourier transform of g_k in the first variable and the RHS of (16) represents a 2-D Fourier transform of f(x,y). The exponent for e contains the expression U(x+yv) which is the inner product of the two vectors (U, Uv) and (x,y). For a constant v, the RHS of (15) is thus an expression for the line

$$\begin{cases} X = U \\ Y = Uv, \end{cases} \tag{17}$$

in the 2-dimensional Fourier transform of f(x,y).This means that

$$[F^{[1]}g_k]\ (U,\ v) = [F_2Q^{-k}f]\ (U,\ Uv). \tag{18}$$

This is the "projection slice theorem" stated in linogram form.

For the moment we leave (18) and start at another end, namely the selfevident fact that

$$f(x,y) = \int_{-\infty}^{\infty}\int [F_2f]\ (X,Y)\ e^{i2\pi(x,y)(X,Y)}\ dX\ dY, \tag{19}$$

i.e. if we make an inverse Fourier transform of the Fourier transform of f(x,y), of course we regain f(x,y).

Change from coordinates (X,Y) to polar coordinates (R,Θ) in the Fourier domain. The usual integration in Θ from 0 to 2π is replaced by the equivalent range from -π/4 to 7π/4.

$$f(x,y) = \int_{-\pi/4}^{7/4\pi} \int_{0}^{\infty} [F_2f]\ (R\cos\Theta,\ R\sin\Theta) e^{i2\pi(x,y)(R\cos\Theta,R\sin\Theta)} |R|\ d\ R\ d\Theta. \tag{20}$$

If R in (20) with the integration between 0 and ∞ is permitted to be negative and is integrated from $-\infty$ to ∞ it is sufficient with an integration of Θ from 0 to π, that is in (20)

$$\int_{-\pi/4}^{7/4\pi}\int_{0}^{\infty} \text{ is replaced by } \int_{-\pi/4}^{3/4\pi}\int_{-\infty}^{\infty}.$$

Divide the angular range for Θ in the two ranges.

$$-\frac{\pi}{4} \leqslant \Theta < \frac{\pi}{4} \quad \text{and} \quad \frac{\pi}{4} \leqslant \Theta < \frac{3}{4}\pi \,. \tag{21}$$

For each range we will make an inverse transformation of $F_2\underline{f}$, each incomplete and resulting in a partial image $f_k(x,y)$. For the second range in (21) we will rotate f(x,y) clockwise using the operator Q defined in (11). The two partial images will be denoted $f_0(x,y)$ and $f_1(x,y)$ and are defined by

$$f_k(x,y) = \int_{-\pi/4}^{\pi/4}\int_{-\infty}^{\infty} [F_2Q^{-k}f]\,(R\cos\Theta;\, R\sin\Theta)e^{i2\pi(x,y)(R\cos\Theta,\, R\sin\Theta)}|R|\,d\,R\,d\Theta, \tag{22}$$

When the two partial images are added together the result will be a complete image of f(x,y).

$$f(x,y) = \sum_{k=0}^{1} Q^k \int_{-\pi/4}^{\pi/4}\int_{-\infty}^{\infty} [F_2Q^{-k}f]\,(R\cos\Theta,\, R\sin\Theta)e^{i2\pi(x,y)(R\cos\Theta,R\sin\Theta)}|R|d\,R\,d\Theta. \tag{23}$$

or,

$$f(x,y) = \sum_{k=0}^{1} [Q^k f_k]\,(x,y). \tag{24}$$

Note that the two $f_k(x,y)$; k=0,1 are not subject to the same limitations as defined for f(x,y) in (1).

We now change the variables on the RHS of (22) from polar coordinates to the Cartesian coordinates used in (18), so that U = R cosΘ and v = tanΘ. From this follows that

$$Uv = R\sin\Theta, \quad \frac{1}{\sqrt{(1+v^2)}} = \cos\Theta \text{ and } \frac{v}{\sqrt{(1+v^2)}} = \sin\Theta. \tag{25}$$

We than have $dU\sqrt{(1+v^2)} = dR$ and $\frac{dv}{1+v^2} = d\Theta$,

so that $$|U|\, dU\, dv = |R|\, dR\, d\Theta.$$

When these changes are inserted in (23) we get

$$f_k(x,y) = \int_{-1}^{1}\int_{-\infty}^{\infty} [F_2Q^{-k}f]\,(U, Uv)e^{i2\pi(x,y)(U,Uv)}|U|dU\, dv. \tag{26}$$

Compare (26) and (18). The difference between the RHS in 18 and the integrand on the RHS in (26) is that the latter is multiplied by the factor $|U|$. This then constitutes the necessary filtration of the spatial frequencies in the projection data. Define

$$[F^{[1]}g'_k]\,(U,v) = [F_2Q^{-k}f]\,(U,Uv)\;|U|W(|U|),\; -1 \leqslant v < 1 \tag{27}$$

so that the two linograms $g'_k(u,v)$ consist of properly filtrated data. $W(|U|)$ is a band-limiting function.

<u>The linogram algorithm</u>. We are now ready to derive the algorithm. Insert (27) in (26)

$$f_k(x,y) = \int_{-1}^{1}\int_{-\infty}^{\infty}[F^{[1]}g'_k]\,(U,v)e^{i2\pi xU}\,dU\, dv, \tag{28}$$

and perform the inverse transform in U. We then have

$$f_k(x,y) = \int_{-1}^{1} g'_k\,(u,v)\,dv \quad . \tag{29}$$

Change from variabel u to x according to (15).

$$f_k(x,y) = \int_{-1}^{1} g'_k\,(x+yv,v)\,dv \quad . \tag{30}$$

For a constant y-value the LHS is a line through $f_k(x,y)$ parallel to the x-axis and the RHS is a set of parallel line integrals through the filtered

linogram (Fig 5). This may be regarded as a parallel projection of the filtered linogram. We can then use the projection theorem as follows.

A Fourier transform of $f_k(x,y)$ in the first variable may be expressed as

$$[F^{[1]}f_k]\ (X,y) = \int_{-\infty}^{\infty} f_k(x,y)e^{-i2\pi\ Xx}\,dx.$$

Now insert (30) on the RHS.

$$[F^{[1]}f_k]\ (X,y) = \int_{-\infty}^{\infty}\int_{-1}^{1} g'_k\ (x+yv,v)dv\ e^{-i2\pi\ Xx}\,dx \tag{31}$$

As $g_k$is zero for $|v| > 1$ so is g'_k. We can then extend the limits of integration for v to infinity. Change variabel from x to u according to (15).

$$[F^{[1]}f_k]\ (X,y) = \int_{-\infty}^{\infty}\int_{-\infty}^{\infty} g'_k\ (u,v)\ e^{-i2\pi X(u-yv)}dv\ du\ . \tag{32}$$

The RHS represents a 2-dimensional Fourier transform of $g'_k\ (u,v)$. The exponent for e contains X(u-yv), which may be regarded as the inner product of the two vectors

$$(X,\ -yX) \text{ and } (u,v). \tag{33}$$

We then have that

$$[F^{[1]}f_k]\ (X,y) = [F_2\ g'_k]\ (X,-yX). \tag{34}$$

Note the similarity between (34) and (18).

We said that (18) was an expression for the celebrated projection slice theorem, which states that the Fourier transform of a projection of a function is to be found as a central line in the 2-dimensional Fourier transform of the function.

In (34) we have that the Fourier transform of a line in the function, parallel to the x-axis, is to be found as a central line in the 2-dimensional Fourier transform of the filtrated linogram to the function.

Note also that in the 2-dimensional Fourier transform

$[F_2 g'_k]\ (U,V)$ we have that,

$$\begin{cases} U = X \\ V = -yX. \end{cases}$$

The image $f_k(x,y)$ stands in a similar relation to $g'_k\ (u,v)$, as $g_k(u,v)$ to $f_k(x,y)$.

From (34) we get

$$f_k(x,y) = \int_{-\infty}^{\infty} [F_2 g'_k]\ (X, -yX) e^{i2\pi\, xX}\, dX, \tag{35}$$

which says that a line in $f_k(x,y)$ parallel to the x-axis, i.e. with a fixed y-value, is reconstructed by performing an inverse Fourier transform of the values along the line

$$V = -yX \tag{36}$$

in the 2-dimensional Fourier transform of the filtered linogram $g'_k(u,v)$. The final reconstructed image of the object $f(x,y)$ is acquired by rotating $f_1(x,y)$ and adding it to $f_0(x,y)$ according to (24). It is repeated here.

$$f(x,y) = \sum_{k=0}^{1} [Q^k f_k]\ (x,y) \quad . \tag{37}$$

Some comments on implementation

A description of how to implement the linogram method is given in [2] and a comprehensive description of how to implement linograms with the slightly different definition treated here and in [4] is given in [4]. In [4] the result from different kinds of band limiting filters, W(U), were compared with each other and with the results from filtered back projection. For this purpose several phantoms were used. All experiments were simulated with the program package SNARK77. In [4] is also given an excellent description of this program package by which phantoms and a number of different projections and reconstruction methods may be simulated.

An important feature in the implementation is the two-dimensional Fourier transform of the filtered linogram. The first transform in the u-direction can easily be done by FFT of the Linogram. The filtration is then performed by multiplying with $|U|$. If now the transform in the v-direction also is done by FFT we would get a rectangular grid of points as in Fig 6a. From (36) and (1) we see that only points lying in the sectors defined by

$$V = - yX \quad ; \quad |y| \leq 1, \tag{38}$$

are relevant and from these we would have to interpolate in order to get the points shown in fig 6b. For small values of X there are then very few points to interpolate from. The points in fig 6b, however, can be calculated exactly and without interpolation by doing a DFT and this in turn can be calculated by the so called chirp-z-transform (CZT) [7], which performs the DFT at the cost of 3 FFT's.

By the use of CZT it is thus possible to implement the linogram method without any kind of interpolation.

Direct Fourier methods

These are methods in which the image is reconstructed from its two-dimensional Fourier transform by two inverse FFT's.

The two-dimensional Fourier transform for the image is derived from the one-dimensional Fourier transforms of the projections of the object, utilizing the "projection slice theorem". This theorem says that when a parallel projection is Fourier transformed in its first variable, it is equal to a line through the origin of the two-dimensional Fourier transform of the image. When projection data are in the sinogram form defined in (10) they may be denoted $p(r,\Theta)$. Here r is the coordinate along the axis perpendicular to the rays. For sinograms the projection slice theorem is expressed as

$$[F^{[1]}p]\ (R,\Theta) = [F_2 f]\ (R\cos\Theta,\ R\sin\Theta)\ . \qquad (39)$$

For linograms this theorem has already been stated as (18), it is repeated here

$$[F^{[1]}g_k]\ (U,v) = [F_2 f_k]\ (U,\ Uv)\ .$$

As $X = U$, we can rewrite this as

$$[F^{[1]}g_k]\ (X,v) = [F_2 f_k]\ (X,\ Xv)\ . \qquad (40)$$

When data for the LHS in the two expressions (39) and (40) are known for points in a rectangular array, the RHS represents these points on radial lines through the origin.

In the sinogram case the points representing the RHS of (39) lie on a polar grid with equal increments in Θ between the radial lines and equal increments in R between the points on the radial lines.

This polar grid represents points in the two-dimensional Fourier transform of the image but the image cannot be calculated directly from this grid. First we have to change it into a rectangular grid of points and this is done by interpolation from the polar grid. The image can then be reconstructed by a sequence of two one-dimensional inverse FFT's, one parallel to the X-axis and the other to the Y-axis.

A crucial step is the interpolation from polar to rectangular coordinates. A simple bilinear interpolation is not sufficient to achieve a good result. More correct interpolations [8], [9] give results comparable to those performed by filtered back projection.

In the linogram case, for each of the two linograms, the points representing the RHS of (40), form a pattern similar to the grid in fig 6b. The radial lines do not have equal increment in Θ but in v, which represents $\tan\Theta$. On the radial lines the points lie on equal increment in the X-coordinate so that the points lie on straight lines parallel to the Y-axis.

The two grids $[F_2 f_k]$ (X,Xv) can be combined in one grid by rotating the grid $[F_2 f_1]$ (X,Xv) the angle $\pi/2$.

$$\sum_{k=0}^{1} [Q^k F_2 f_k] \text{ (X,Xv)} .$$

We would then have a grid as in fig 7. This grid represent points in the two-dimensional Fourier transform of the complete image. As in the sinogram case a rectangular grid may be interpolated. The image may then be reconstructed by two FFT's as in the sinogram case.

A better way, however, would be to reconstruct each partial image f_k from its own partial grid by doing a two-dimensional inverse Fourier transform of it.

If the discrete points representing $[F_2 f_k]$ (X,Xv) were a perfect rectangular grid in (X,Y)-space, we could have used an inverse FFT algorithm two times, first in the direction of one of the axes than in the direction of the other in order to calculate $f_k(x,y)$. Now this is not the case because even though the X-coordinates for the points conform to the grid lines in a rectangular grid, the Y-coordinates do not. In order to do the inverse transform in the Y-direction we have to do a DFT. But this can be achieved by the chirp-z-transform mentioned on p. 10 [7] at the cost of 3 FFT's.

By this transform it is possible to calculate the correct values for

$[F^{[1]}f_k]$ (X,y), without interpolation. We then have to start with the filtered linograms defined in (27) and here restated. As the Fourier variable U is equal to X, U is replaced with X.

$$[F^{[1]}g'_k] (X,v) = [F^{[1]}g_k] (X,v) \; |X| \; W (X) \; . \tag{41}$$

The filtered linogram (the LHS of 41) is then remapped as grid points in the two-dimensional Fourier transform of f_k.

$$[F_2 f_k] (X,vX) = [F^{[1]}g'_k] (X,v) \quad . \tag{42}$$

The next step is to use the CZT to do an inverse DFT in the second variable.

$$[F^{[1]}f_k] (X,y) = [(F^{[2]})^{-1} \; F_2 f_k] (X,vX) \tag{43}$$

We can then calculate $f_k(x,y)$ by doing an inverse FFT in the first variable. The complete image is then calculated by (24).

Comparison between the Linogram method (LM) and the Direct Fourier Method with Linograms (DFM). In both methods the steps are the same up to the stage where we have filtered linograms which are Fourier transformed in the first variable, i.e. $[F^{[1]}g'_k] (X, v)$.

From this point they take different routes (Fig 8) and arrive at the same result, namely a partial image Fourier transformed in its first variable, i.e. $[F^{[1]}f_k] (X, y)$.

In both methods all operations are only in the second variable, which is transformed from v to y. The first variable is all the time X.

In the LM a Fourier transform of the linogram in the v-coordinate is carried out by CZT, which changes this coordinate into V, expressed as -yX. A multiplication of this coordinate with (-1/X) is then performed, which gives the desired result.

In the DFM the linogram is first remapped into the 2-dimensional Fourier transform of the partial image. The v-coordinate is multiplied with X which

changes it into Y. An inverse Fourier transform by CZT in this coordinate then gives the desired result.

Although the two methods are conceptually different the calculations are practically identical. Both methods arrive at exactly the same result and no interpolations are performed.

This is clear from the following. Assume that we only compute one column in $[F^{[1]}f_k]$ (X,y), (i.e. in the following X < 1 and is a constant). Call this sequence of values I(y). It is computed from a corresponding column of values in $[F^{[1]}g'_k]$ (X,v) (with the same constant X). Call this sequence L(v).

In the Linogram method we make a forward Fourier transform into a new sequence $[F_2 g'_k]$ (X,V). We do not, however, compute this sequence for integer values of V but at the fractional values for which V = -yX

$$\left[F_2 g'_k\right](X,-yX) = N^{-1} \sum_{n=\frac{N-1}{2}}^{\frac{N-1}{2}} L(v) e^{-i2\pi \frac{(-yX)v}{N} n}$$

$$= N^{-1} \sum_{n=\frac{N-1}{2}}^{\frac{N-1}{2}} L(v) e^{i2\pi \frac{yXv}{N} n}$$

The "remapping" of the LHS into I (y) consists in letting the second variable assume integer values. As the LHS in fact only is a sequence of values, it can directly be accepted as I (y).

The "remapping step" is therefore only a conceptual step. It is no step in the calculations. So we have that

$$I(y) = N^{-1} \sum_{n=\frac{N-1}{2}}^{\frac{N-1}{2}} L(v) e^{i2\pi \frac{yXv}{N} n}$$

In the Direct Fourier method we start with a similar conceptual "remapping step" by considering the sequence L(v) to be values at the fractional coordinate points Y = vX, in $[F_2 f_k]$ (X,vX).

We then do an inverse Fourier transform of this sequence resulting in I (y)

$$I(y) = N^{-1} \sum_{n=\frac{N-1}{2}}^{\frac{N-1}{2}} \left[F_2 f_k\right](X, vX) e^{i2\pi \frac{yXv}{N} n}$$

$$= N^{-1} \sum_{n=\frac{N-1}{2}}^{\frac{N-1}{2}} L(v) e^{i2\pi \frac{yXv}{N} n}$$

Thus the calculations are exactly the same for both methods.

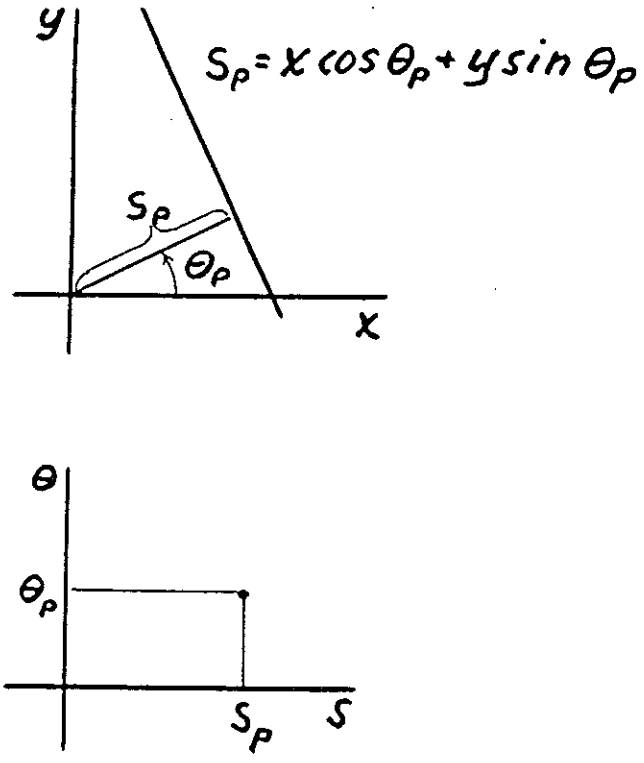

Fig 1. A line specified by the point (s_p, Θ_p).

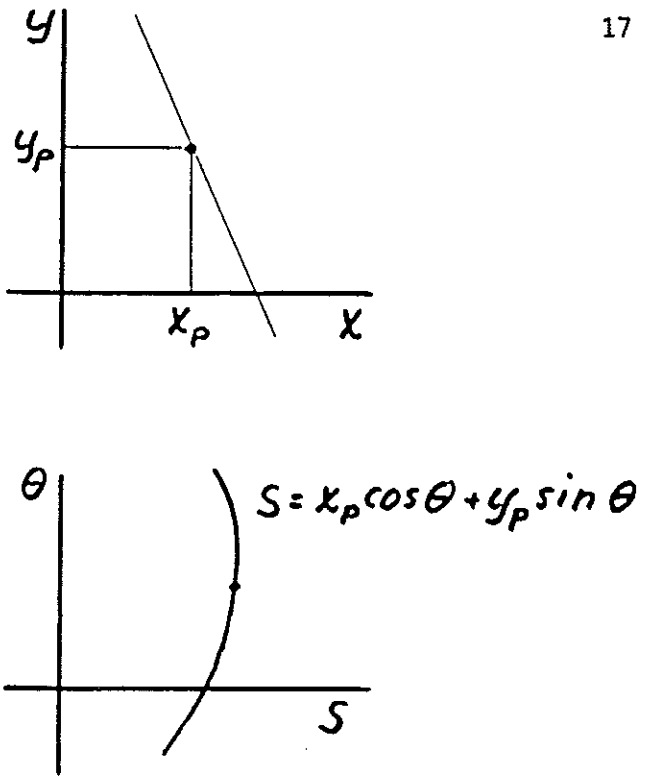

Fig 2. A sinusoid (only a part of it is shown), specified by the point (x_p, y_p).

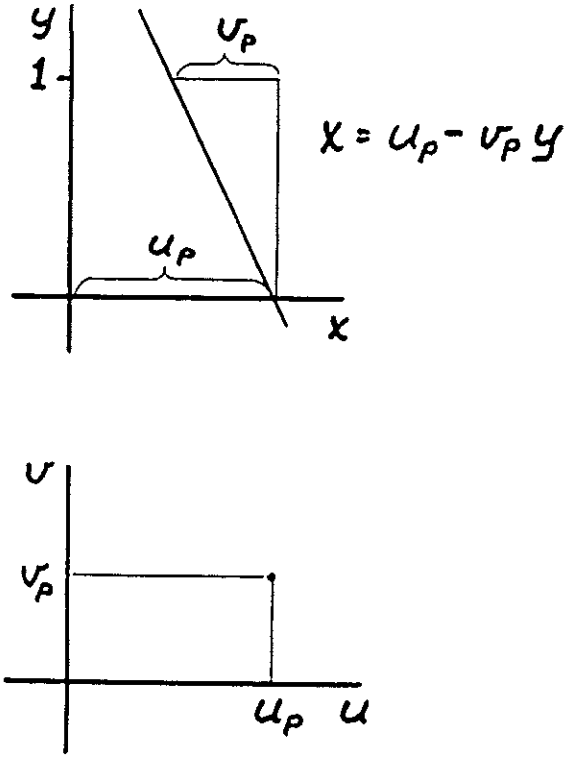

Fig 3. A line specified by the point (u_p, v_p).

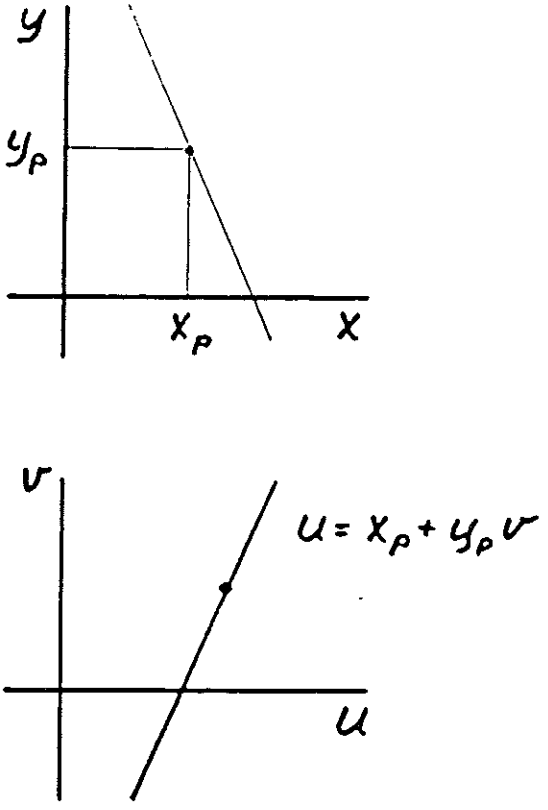

Fig 4. A line specified by the point (x_p, y_p).

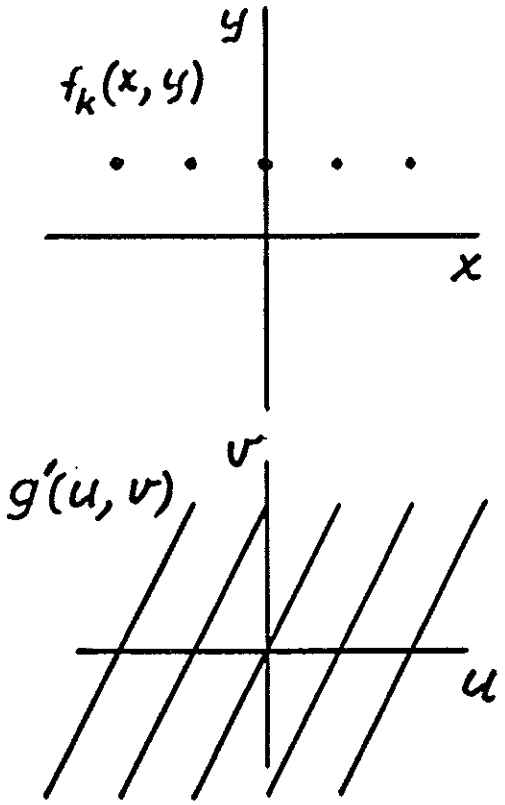

Fig 5. The row of points in $f_k(x,y)$ parallel to the x-axis are reconstructed by a parallel projection of $g'(u,v)$.

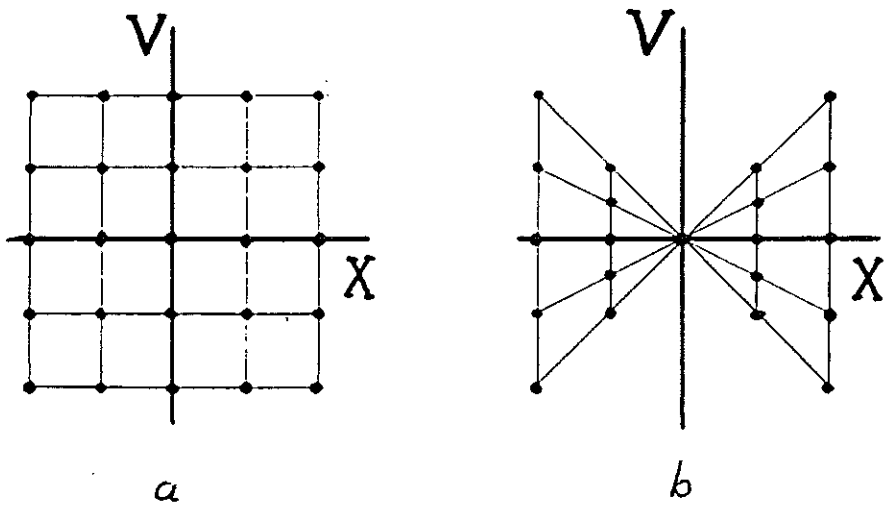

Fig 6. a) The resulting grid if the Fourier transform in the v-direction is performed by FFT. b) The grid of points needed for the reconstruction. This grid can be achieved without interpolation by CZT.

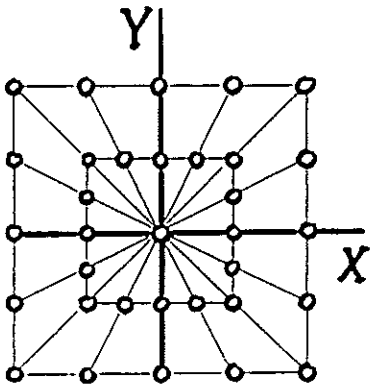

Fig 7. The grid resulting from a remapping and combination of the two $[F^{[1]}{}_{g'_k}]$ (X,v).

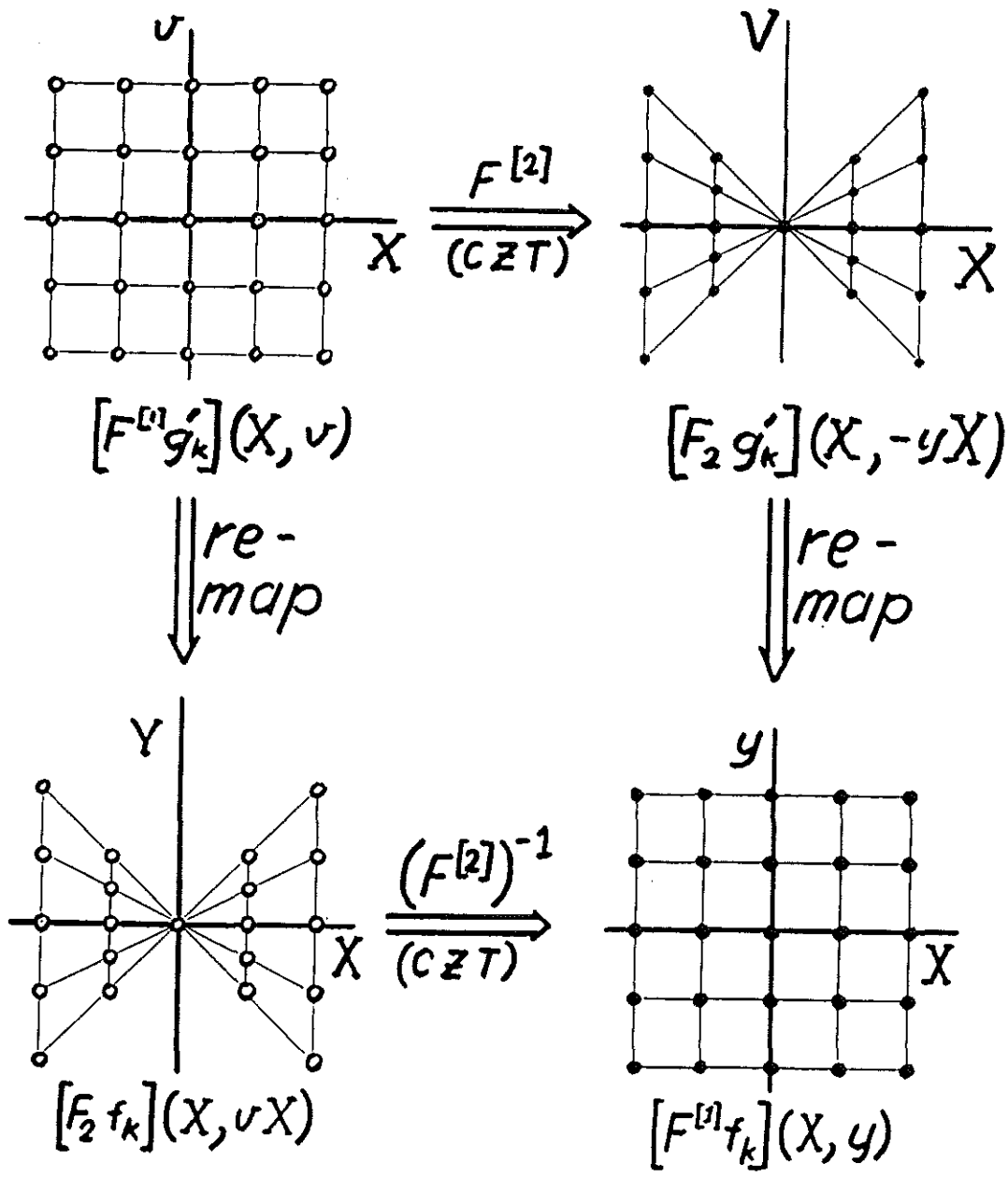

Fig 8. Pictorial comparison of the different routes taken by the Linogram Method and the Direct Fourier Method with linograms. Both start from a filtered and Fourier transformed linogram (upper left) and end at a partial image Fourier transformed in its first variable (lower right). The Linogram Method goes via the 2-D Fourier transformed linogram (upper right), the Direct Fourier Method via the 2-D Fourier transformed image (lower left).

REFERENCES

[1] P.R. Edholm and G.T. Herman, "Linograms in image reconstruction from projections", IEEE Trans. Med. Imaging, vol MI-6, pp 301-307, 1987.

[2] P.R. Edholm, G.T. Herman and D. Roberts, "Image reconstruction from linograms: Implementation and evaluation", IEEE Trans. Med. Imaging, vol MI-7, pp 239-246, 1988.

[3] P.R. Edholm, "Linograms", Report ULi-RAD-R-058, University of Linköping.

[4] M. Magnusson, "Implementation of the linogram method for CT-reconstruction", in preparation.

[5] L. Axel, G.T. Herman, J. Listerud and D. Roberts, "Magnetic resonance imaging based on linograms", in preparation.

[6] This term was introduced in a poster presentation at the 1975 meeting on Image Processing for 2-D and 3-D Reconstructions from Projections at Stanford, CA. The material appeared in a collection of postdeadline papers for that meeting. PD5 - Tomogram Construction by Photographic Techniques. Paul Edholm and Bertil Jacobsson.

[7] L.R. Rabiner, R.W. Schafer and C.M. Rader, "The chirp-z-transform algorithm", IEEE Trans. Audio Electroacoust., Vol. AU-17, pp. 86-92, 1969.

[8] H. Stark, J.W. Woods, I. Paul and R. Hingorani, "An investigation of computerized tomography by direct Fourier inversion and optimum interpolation, IEEE Trans. Biomed. Eng., Vol. BME-28, pp. 496-505, 1981.

[9] F. Natterer, "Fourier reconstruction in tomography", Numer. Math. Vol. 47, pp. 343-353, 1985.

[10] G.T. Herman and S.W. Rowland, "SNARK77": A programming system for image reconstruction from projections", Dep. Comput. Sci., State Univ. New York at Buffalo, Tech. Rep. 130, 1978.

Utgivna rapporter vid Radiofysiska Institutionen, Universitetet i Linköping

1. Leif Kusoffsky: **MTF-begreppet och dess applikation.** (1973-05-23)
2. Bengt Nielsen: **Undersökning av uranraster.** (1973-06-15)
3. Per Spanne: **High dose RPL-dosimetry.** (1973-09-30)
4. har utgått! Är ersatt av rapport 041.
5. Carl Carlsson: **Spridd strålning i röntgendiagnostik.** (1973-09-10)
6. Leif Kusoffsky och Carl Carlsson: **Modulationsöverföringsfunktionen, MTF.** (1973-09-12)
7. har utgått! Är ersatt av rapport 052.
8. Carl Carlsson: **Grundläggande fysik inom röntgendiagnostik.** (1973-09-14)
9. Paul Edholm: **Bildbehandling.** (1973-09-20)
10. har utgått! Är ersatt av rapport 026.
11. Bengt Nielsen: **Investigation of Roentgen Focal Spot.** (1973-11-12)
12. Gudrun Alm Carlsson: **Kärnfysikaliska grunder för radioaktiva nuklider.** (1974-11-11)
13. Carl Carlsson: **Strålningsdosimetri med radioaktiva nuklider i människa.** (1974-11-13)
14. Carl Carlsson: **Växelverkan mellan materia och joniserande strålning från radioaktiva nuklider.** (1974-11-29)
15. Per Spanne: **Strålningsdetektorer.** (1974-11-29)
16. Gudrun Alm Carlsson: **Statistisk precision vid radioaktivitetsmätning.** (1974-12-05)
17. Carl Carlsson: **Aktivitetsbestämning ur uppmätt räknehastighet.** (1974-12-05)
18. Gudrun Alm Carlsson: **Pulshöjdsanalys.** (1974-12-12)
19. Gudrun Alm Carlsson: **Kvantelektrodynamik för elektroner - Feyman-diagram och strålningskorrektion för tvärsnitt.** (1975-01-07)
20. Gudrun Alm Carlsson: **Klassisk elektrodynamik. Växelverkan mellan laddade partiklar och elektromagnetiska fält.** (1975-01-07)
21. Sten Carlsson: **Vätskescintillatorn.** (1975-01-09)
22. Per Spanne och Gudrun Alm Carlsson: **Problem vid radioaktivitetsmätningar vid höga räknehastigheter.** (1975-01-21)
23. Carl Carlsson: **Signal och bakgrund vid mätning av låga radioaktiviteter.** (1975-02-24)
24. Bertil Persson: **Val av radionuklider och radioaktiva markörer för användning in vivo.** (1975-03-17)
25. Carl Carlsson: **Användning av logaritmer och exponetialfunktioner inom röntgendiagnostik.** (1975-04-03)

26. Ulf Boström: **Röntgenbildförstärkare och Röntgen-TV.** (1975-04-07) (Ersätter rapport nr 010).
27. Gudrun Alm Carlsson: **Riskuppskattningar vid små stråldoser och strålskyddsrekomendationer.** (1975-04-10)
28. Gudrun Alm Carlsson: **Analys av Monte Carlo metoder för simulering av fotontransporter.** (1975-09-12)
29. Leif Kusofsky: **Rutinbeskrivningar. Monte Carlo program för fotontransportsimuleringar.** (1975-09-05)
30. Leif Kusoffsky: **Jämförelse mellan två olika växelverkansmodeller för 15-200 keV fotoner använda i Monte Carlo beräkningar av spridd strålning.** (1975-09-12)
31. Gudrun Alm Carlsson: **A critical analysis of concepts of ionizing radiation and absorbed dose.** (1977-01-21)
32. Gudrun Alm Carlsson: **A different formulation of the definition of energy imparted.** (1977-01-21)
33. Carl Carlsson: **Vectorial and plane energy fluences - useful concepts in radiation physics.** (1977-06-01)
34. Gudrun Alm Carlsson och Carl Carlsson: **Strålningsdosimetri i röntgendiagnostiken.** (1979-10-01)
35. Gudrun Alm Carlsson: **Absorbed dose equations. The general solution of the absorbed dose equation and solutions under different kinds of radiation equilibrium.** (1978-01-27)
36. har utgått! Är ersatt av 057.
37. Paul Edholm: **Konturen. En radiologisk studie.** (1978-05-10)
38. Gudrun Alm Carlsson: **Burlins kavitetsteori.** (1979-08-15)
39. Bengt Nielsen: **Upplösningförmåga, oskärpa och MTF.** (1980-01-23)
40. Gudrun Alm Carlsson, Karl-Fredrik Berggren, Carl Carlsson och Roland Ribberfors: **Beräkning av spridningstvärsnitt för ökad noggrannhet i diagnostisk radiologi. I Energibreddning vid Comptonspridning.** (1980-01-25)
41. Paul Edholm: **Röntegenprojektionens geometri.** (1980-09-05) (Ersätter rapport 004)
42. Per Spanne och Carl Carlsson: **Kontroll av kärnkraftsindustrins TLD-system för persondosimetri.** (1980-10-30)
43. Gudrun Alm Carlsson: **Kavitetsteori - allmänna grunder.** (1981-01-20)
44. Carl Carlsson och Bengt Nielsen: **Kvalitetsvärdering av raster för bekämpning av spridd strålning vid röntgenundersökningar. Del I Teori** (1981-08-21)

45. Carl Carlsson och Bengt Nielsen: **Kvalitetsvärdering av raster för bekämpning av spridd strålning vid röntgenundersökningar. Del II Experimentella resultat.** (1981-08-21)
46. Bengt Nielsen: **Mätmetoder för att bestämma modulationsöverförings-funktionen för radiologiska system.** (1981-08-21)
47. Gudrun Alm Carlsson: **Skalära och vektoriella fysikaliska storheter. Deras betydelse för förståelsen av röntgendetektorernas uppträdande i ett strålningsfält.** (1981-09-23)
48. Gudrun Alm Carlsson: **Fotonspridningsprocessen vid röntgendiagnostiska strålkvaliteter.** (1981-09-23)
49. Gudrun Alm Carlsson: **Effective use of Monte Carlo methods for simulating photontransport with special reference to slab penetration problems in X-ray diagnostics.** (1981-10-19)
50. Anders Björk och Bengt-Olof Dahl: **Konstruktion av experimentell datortomograf. Utarbetande av datorproigram för styrning av rörelseenheter, insamlande av mätdata och presentation av bilder.** (1982-06-23)
51. Georg Matscheko: **Utnyttjande av Comptonspridning vid bestämning av primärspektrum av röntgenstrålning från diagnostiska röntgenrör.** (1982-11-12)
52. Paul Edholm: **Praktisk tomografi.** (1982-12-08)
53. Sune Eriksson, Carl Carlsson, Olof Eckerdahl och Jüri Kurol: **Riktlinjer för klinisk och röntgenologisk övervakning av överkäkshörntändernas eruption hos barn och ungdomar mellan 8 och 15 år. Analys av indikationer och metoder för röntgenundersökning med hänsyn tagen till stråldoser och diagnostisk utfall (december 1984)**
54. Paul Edholm: **Diagnostisk radiologi för propedeutkursen.** (1985-01-31)
55. Börje Forsberg och Per Spanne: **Stråldoser till personal vid kliniker för gynekologisk onkologi.** (1985-10-15)
56. Paul Edholm och Bernt Lindholm: **En ny metod för fotografisk utjämning samt en lättskött apparat.** (1986-09-15)
57. Gudrun Alm Carlsson och Carl Carlsson: **Riskuppskattningar och strålskyddsrekomendationer - Vår strålningsmiljö. Kompendium i strålningshygien.** (1988-01-20) (Ersätter 036)
58. Paul Edholm: **Linograms.** (1988-11-24)
59. Gudrun Alm Carlsson, David Dance och Jan Persliden: **Grids in mammography: Optimization of the information content relative to radiation risk.** (1989-08-31)
60. Paul Edholm: **Diagnostisk radiologi för propedeutkursen.** (1990-01-22) (Ersätter rapport 054)

61. har utgått! Är ersatt av rapport 065.
62. Michael Sandborg och Gudrun Alm Carlsson: **Beskrivning av de artificiella parametrarna vid EGS4 Monte Carlo simuleringar och deras inverkan på absorberade djupdoser från elektroner i vatten.** (1990-05-09)
63. Michael Sandborg och Gudrun Alm Carlsson: **Jämförelse mellan ett niobfilter (NIOBI-X) och konventionell filtrering vid skärmfilm radiografi. Inverkan på primärspektrum, kontrast, rörbelastning och strålrisk.** (1990-05-09)
64. Frantisek Pernicka, Carl Carlsson, Eva Lund: **Experimental Determination of the Angular Response of the Directional dose equivalent H'(10) for 137-Cs gammarays and ISO-narrow X-ray spectra. (1991-01-31)**
65. Paul Edholm: **The Linogram Algorithm and Direct Fourier Method with Linograms.** (1991-01-31) Ersätter R-061.
66. Carl Carlsson: **Differences in reported backscatter factors, BSF, for low energy X-rays. A literature study.** (1991-01-31).
67. Eva Lund: **Free Radical Dosimetry, especially Electron Spin Resonance analysis of radiation induced free radicals i L-α-alanine.** (1991-03-01).